Circuits, Systems, and Signal Processing
https://doi.org/10.1007/s00034-024-02691-5

Complex-Valued Noisy Sinewaves Frequency Estimator Based on DTFT Linearization and Interpolation

Daniel Belega[1] · **Dario Petri**[2]

Received: 28 October 2022 / Revised: 8 April 2024 / Accepted: 9 April 2024

Abstract
This paper proposes an Interpolated Discrete-Time Fourier Transform (LIpDTFT) estimator for complex-valued noisy sinewave frequency based on the Linearization of the DTFT module behavior around the spectrum peak. It belongs to a class of LIpDTFT estimators that compensate the poor Discrete Fourier Transform (DFT) frequency resolution by interpolating two DTFT samples located very close to an initial frequency estimate. As compared with other DTFT-based frequency estimators recently proposed in the literature, the proposed LIpDTFT estimator ensures a smaller interpolation error and a lower processing effort. Moreover, if the rectangular window is adopted, it almost attains the unbiased Cramér-Rao Lower Bound (CRLB) even if a very small number of samples is analyzed. The accuracies ensured in different operating conditions by the proposed frequency estimator and other state-of-the-art DTFT-based algorithms are compared to each other through computer simulations.

Keywords Complex-valued sinewave · Discrete-time Fourier transform · Frequency estimation · Interpolation · Statistical analysis

1 Introduction

Many application fields such as communications and radar signal processing require accurate and real-time estimation of the frequency of complex-valued noisy sinewaves [7, 19, 25, 28]. The so-called Interpolated Discrete-Time Fourier Transform (IpDTFT)

✉ Daniel Belega
daniel.belega@upt.ro

Dario Petri
dario.petri@unitn.it

1 Department of Measurements and Optical Electronics, Politehnica University Timişoara, Bv. V. Pârvan, Nr. 2, 300223 Timişoara, Romania

2 Department of Industrial Engineering, University of Trento, 38123 Trento, Italy

Published online: 03 May 2024

algorithms can be advantageously employed to estimate the signal frequency due to their high accuracy and low computational burden. They are two steps algorithms: at first a coarse frequency estimate is obtained as the index of the highest DFT spectrum sample, then a fine frequency estimate is derived by interpolating DTFT samples located very close to the DFT spectrum peak. The aim of this second step is to compensate the so-called picket-fence effect due to the finite number of processed samples, so determining the inter-bin frequency location [22]. The IpDTFT fine frequency estimators proposed in the literature are based on two [1–3, 14, 17, 22, 24, 26, 29] or more DTFT samples [4, 8, 9, 11, 12, 14, 16, 20, 23, 30] and an iterative procedure may be employed. Some algorithms weight the input signal by using a suitable window function in order to reduce the contribution on the estimated frequency of the spectral interference from possible disturbing tones (such as harmonics and interharmonics) [13]. The Maximum Sidelobe Decay (MSD) windows are often employed due to both their optimal spectral leakage reduction capabilities [21] and the simplicity of the analytical expressions involved in the DTFT samples interpolation [4].

The classical Interpolated Discrete Fourier Transform (IpDFT) frequency estimator interpolates the two highest DFT samples [2, 3, 22, 24, 26]. It is very simple and very fast, but the variance of the related estimator does not attain the unbiased Cramér-Rao Lower Bound (CRLB) [27] when the analyzed sinewave is affected by wideband noise. To overcome this problem an iterative two-point IpDTFT frequency estimator based on the rectangular window, called in the following the AM algorithm, has been proposed in [1]. In each iteration, two DTFT samples located $\pm$ 0.5 bins apart from the highest DTFT sample are interpolated; two iterations suffice to almost attain the CRLB. A generalization of that algorithm, in which the two interpolation points are shifted by $\pm q$ bins ($-0.5 \leq q < 0.5$) with respect to the highest DTFT sample has been proposed in [29]. That algorithm, called q-shift (QS) estimator slightly outperforms the AM algorithm [1] when an appropriate value for q is selected, the number of analyzed samples is enough high, and at least three iterations are performed. Furthermore, a version of the AM frequency estimator that exhibits a smaller bias has been derived in [16], while an extension to cosine windows has been proposed in [6].

A non-iterative three-point IpDFT frequency estimator based on the rectangular window has been proposed in [14]. Its accuracy has been comprehensively analyzed in [8, 9], and its extension to cosine windows has been proposed in [4]. However, the variance of that estimator does not attain the CRLB. Recently, two iterative three-point IpDTFT frequency estimators based on the highest DFT sample and two DTFT samples located at $\pm$ 0.5 bins or $\pm p$ bins ($0 < p \leq 1$) apart have been proposed in [11] and [12], by adopting the rectangular window or an MSD window, respectively. When the rectangular window is adopted, two iterations are enough to almost attain the unbiased CRLB.

A two-step three-point Parabolic Interpolated DTFT (PIpDTFT) frequency estimator has been proposed in [10]. The first step estimates the inter-bin frequency location by applying the three-point IpDFT algorithm [9], while the second step improves the estimation accuracy through a parabolic interpolation of three DTFT points located very close to the estimate returned by first step. An analytical expression for the PIpDTFT estimator interpolation error has been derived in [5] and it has been shown that a suitable selection of the interpolation points allows to almost attain the CRLB.

Also, in [5] the algorithm has been extended to MSD windows and it has been shown that the simpler classical two-point IpDFT algorithm [22, 24, 26] can be used to estimate the initial frequency with no effect on the final accuracy.

This paper is aimed at the derivation of a three-step two-points IpDTFT (LIpDTFT) frequency estimator based on the Linearization of the DTFT module behavior around the spectrum peak. The first step returns a coarse frequency estimate as the index of the highest DFT spectrum sample. In the following step a first estimate for the inter-bin frequency location is obtained by applying the classical two-point IpDFT algorithm [22, 24, 26]. The last step improves the estimation accuracy by linearizing the behavior of the DTFT module and interpolating two DTFT samples located at frequencies very close to estimate obtained from the two previous steps. The proposed LIpDTFT algorithm ensures both a smaller interpolation error and a lower processing effort than the PIpDTFT algorithm. The effect of windowing on estimation accuracy is also analyzed in the paper. The accuracies of the LIpDTFT, the PIpDTFT and other state-of-the-art interpolated DTFT frequency estimators are compared to each other by means of computer simulations.

The remaining of this paper is organized as follows. In Sect. 2 the proposed LIpDTFT frequency estimator is derived, then its interpolation error is analyzed in Sect. 3. A performance comparison with state-of-the-art interpolated DTFT frequency estimators is then performed in Sect. 4. Section 5 concludes the paper.

2 The proposed LIpDTFT estimator

Let's consider a noisy complex-valued sinewave, modelled as:

$$y(m) = Ae^{j(2\pi f m+\phi)} + e(m), \quad m = 0, 1, 2, \ldots, M-1 \tag{1}$$

where A, f, and ϕ are the amplitude, the normalized frequency, and the initial phase of the sinewave, $e(\cdot)$ is a complex-valued additive white Gaussian noise with zero mean and variance σ^2, and M is the record length. The Signal-to-Noise Ratio (SNR) of (1) is $SNR = \frac{A^2}{\sigma^2}$.

The normalized frequency f can be expressed as:

$$f \stackrel{\text{def}}{=} \frac{\nu}{M} = \frac{l+\delta}{M}, \tag{2}$$

where $\nu = l + \delta$ represents the number of acquired sinewave cycles or the normalized frequency expressed in bins; l is its integer part and δ ($-0.5 \leq \delta < 0.5$) is the inter-bin frequency location.

The DTFT of signal (1) is:

$$Y(\lambda) \stackrel{\text{def}}{=} \sum_{m=0}^{M-1} y(m)e^{-j2\pi\frac{\lambda}{M}m} = AW(\lambda-\nu)e^{j\phi} + E(\lambda), \quad \lambda \in [0, M) \tag{3}$$

where $W(\lambda) = \frac{\sin(\pi\lambda)}{\sin\left(\frac{\pi\lambda}{M}\right)} e^{-j\pi\frac{M-1}{M}\lambda}$ and $E(\lambda)$ are the DTFTs of the rectangular window $w(\cdot)$ that models the signal truncation, and wideband noise $e(\cdot)$, respectively.

For the sake of notation, the window DTFT module is represented as $|W(\lambda)| \triangleq \widetilde{W}(\lambda)$, while the DTFT interpolation points are denoted as $P_{-1} \triangleq \left|Y\left(\hat{\nu}_0 - d_x\right)\right|$, $P_0 \triangleq \left|Y\left(\hat{\nu}_0\right)\right|$, and $P_{+1} \triangleq \left|Y\left(\hat{\nu}_0 + d_x\right)\right|$, where $\widehat{\nu}_0$ is an initial estimate for the number of observed sinewave cycles ν and d_x ($0 < d_x < 1$) is a fractional shift with respect to the initial frequency estimate. By neglecting the noise contribution, from (3) it follows:

$$P_{-1} \cong A\widetilde{W}(d_x - \Delta\nu_0), \tag{4a}$$

$$P_0 \cong A\widetilde{W}(\Delta\nu_0), \tag{4b}$$

$$P_{+1} \cong A\widetilde{W}(d_x + \Delta\nu_0), \tag{4c}$$

where $\Delta\nu_0 \stackrel{\text{def}}{=} \widehat{\nu}_0 - \nu$ is the error of the initial frequency estimate. In the following we assume that $|\Delta\nu_0|$ is small, as it often occurs when $\widehat{\nu}_0$ is returned by the classical IpDTFT algorithm [22, 24, 26]. Thus, (4) is accurately approximated by considering only the lower order terms of the Taylor's series:

$$P_{-1} \cong A\widetilde{W}(d_x) - A\widetilde{W}'(d_x)\Delta\nu_0 + \frac{A\widetilde{W}''(d_x)}{2}\Delta^2\nu_0 - \frac{A\widetilde{W}'''(d_x)}{6}\Delta^3\nu_0 + \cdots, \tag{5a}$$

$$P_0 \cong A\widetilde{W}(0) + \frac{A\widetilde{W}''(0)}{2}\Delta^2\nu_0 + \cdots, \tag{5b}$$

$$P_{+1} \cong A\widetilde{W}(d_x) + A\widetilde{W}'(d_x)\Delta\nu_0 + \frac{A\widetilde{W}''(d_x)}{2}\Delta^2\nu_0 + \frac{A\widetilde{W}'''(d_x)}{6}\Delta^3\nu_0 + \cdots, \tag{5c}$$

where $\widetilde{W}'(\cdot)$, $\widetilde{W}''(\cdot)$, and $\widetilde{W}'''(\cdot)$ represents the first, second, and third derivatives of$\widetilde{W}(\cdot)$, respectively. In particular: $\widetilde{W}(0) = M$ and $\widetilde{W}''(0) = -\frac{\pi^2(M^2-1)}{3\cdot M}$, while $\widetilde{W}'(0) = 0$ and $\widetilde{W}'''(0) = 0$ since $\widetilde{W}(\lambda)$ is an even function of frequency.

From (5), by considering only the first order terms and using simple algebra, the following class of two-point LIpDTFT estimators can be derived:

$$\hat{\nu}_{2l\_g} = \hat{\nu}_0 + f\left(\frac{P_i}{P_j}\right), \quad i, j \in \{-1, 0, +1\}, \quad i \neq j, \tag{6}$$

where $f(\cdot)$ is a suitable function of the ratio between two different DTFT samples P_i/P_j, where $i, j \in \{-1, 0, +1\}$.

In the following, the two-point LIpDTFT frequency estimator, defined by:

$$\hat{\nu}_{2l} = \hat{\nu}_0 + \frac{\widetilde{W}(d_x)}{\widetilde{W}'(d_x)}\frac{1 - \frac{P_{+1}}{P_{-1}}}{1 + \frac{P_{+1}}{P_{-1}}}, \tag{7}$$

is analysed since simulations showed that it is the most accurate estimators within those identified by (6).

It is worth noticing that (7) holds for a generic window and the coefficient $\widetilde{W}(d_x)/\widetilde{W}'(d_x)$ can be determined a priori once the fractional shift d_x is fixed.

3 Interpolation Error of the LIpDTFT Frequency Estimator

In this Section an analytical expression of the interpolation error of the LIpDTFT frequency estimator (7) is firstly derived in the case of the rectangular window and considering a noiseless complex-valued sinewave. That error is then compared with the one introduced by the PIpDTFT estimator using both theoretical and simulation results.

By replacing in (7) the expressions of $\widetilde{W}(d_x)$ and $\widetilde{W}'(d_x)$ it results the following expression for the LIpDTFT frequency estimator:

$$\hat{\nu}_{2l} = \hat{\nu}_0 + \frac{\widetilde{W}(d_x)}{\widetilde{W}'(d_x)} \frac{1 - \frac{P_{+1}}{P_{-1}}}{1 + \frac{P_{+1}}{P_{-1}}} = \hat{\nu}_0 + \frac{1}{\pi} \frac{\tan(\pi d_x)\tan\left(\frac{\pi d_x}{M}\right)}{\tan\left(\frac{\pi d_x}{M}\right) - \frac{1}{M}\tan(\pi d_x)} \frac{1 - \frac{P_{+1}}{P_{-1}}}{1 + \frac{P_{+1}}{P_{-1}}}, \tag{8}$$

where $\widetilde{W}(d_x) = \frac{\sin(\pi d_x)}{\sin\left(\frac{\pi d_x}{M}\right)}$ and $\widetilde{W}'(d_x) = \frac{\pi\cos(\pi d_x)\sin\left(\frac{\pi d_x}{M}\right) - \frac{\pi}{M}\sin(\pi d_x)\cos\left(\frac{\pi d_x}{M}\right)}{\sin^2\left(\frac{\pi d_x}{M}\right)}$.

The following Proposition holds (see the proof in the Appendix):

Proposition 1 The interpolation error of the LIpDTFT frequency estimator (7) is given by:

$$\Delta\nu_{2l} = \hat{\nu}_{2l} - \nu \cong \left(-\frac{\pi^2}{15} + \frac{43\pi^4 d_x^2}{1800}\right)\Delta^3\nu_0. \tag{9}$$

Conversely, the interpolation error of the PIpDTFT estimator [10]:

$$\widetilde{\nu}_{3p} = \hat{\nu}_0 - \frac{d_x}{2}\frac{P_{+1} - P_{-1}}{P_{-1} - 2P_0 + P_{+1}}. \tag{10}$$

can be expressed as follows (see the proof in the Appendix):

Proposition 2 The interpolation error of the PIpDTFT frequency estimator (10) is given by:

$$\Delta\nu_{3p} \cong \frac{\pi^2 d_x^2}{20}\Delta\nu_0. \tag{11}$$

From (9) and (11) it follows that:

- when d_x is enough small, the LIpDTFT interpolation error (9) is almost constant, while the PIpDTFT interpolation error (11) strongly depends on the fractional shift d_x;

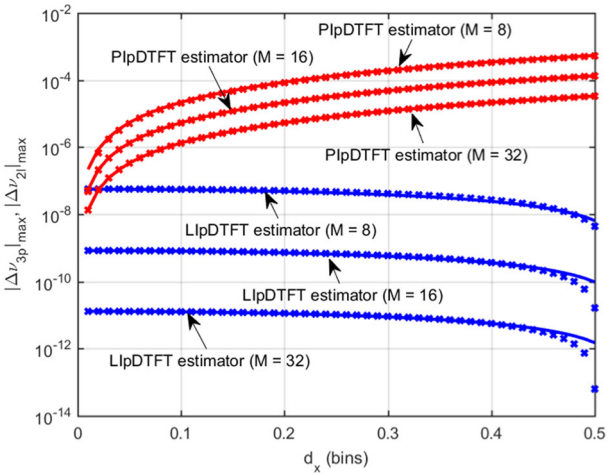

Fig. 1 Noiseless complex-valued sinewaves: maximum magnitude of the LIpDTFT and the PIpDTFT interpolation error versus the fractional shift d_x in bins. 1000 runs of $M = 8$, 16 or 32 samples for each value of d_x with sinewave phase chosen at random. Simulation (crosses) and theoretical (continuous line) results

- since in practice the error $\Delta\nu_0$ is usually negligible with respect to the fractional shift d_x, the LIpDTFT interpolation error is much smaller than the PIpDTFT interpolation error.

In Fig. 1 the magnitude of the maximum interpolation error $|\Delta\nu_{2l}|_{max}$ and $|\Delta\nu_{3p}|_{max}$ returned respectively by the LIpDTFT and the PIpDTFT estimators is reported as a function of the fractional shift d_x, which takes values in the range [0.01, 0.5] bins with a step of 0.01 bins. $\nu = 2.3$ cycles of a noiseless sinewave with amplitude $A = 1$ p.u. are considered, and 1000 runs of $M = 8$, 16, or 32 samples each with phase ϕ chosen at random in the range $[0, 2\pi)$ rad are performed. The integer part l of the number of observed cycles is obtained through a peak search procedure applied to the DFT square module. The initial value for the inter-bin frequency location is obtained by the classical two-point IpDFT algorithm based on the rectangular window [24]. Theoretical results returned by (9) and (11) are also reported in Fig. 1.

As expected, Fig. 1 shows that the LIpDTFT estimator is more accurate than the PIpDTFT estimator if the fractional shift d_x is not too small, which perfectly agree with the behavior expected from the theory. Also, when d_x is smaller than about 0.3 bins, the LIpDTFT interpolation error is almost constant. Observe that the accuracies of both estimators increase as M increases due to the higher accuracy of the initial frequency estimate.

4 Accuracy Comparison with State-of-the-Art Estimators

In this Section the accuracies of the LIpDTFT, the PIpDTFT, the three-point IpDFT estimator [8] (called here the Candan estimator), the AM estimator [1], the QS estimator [29], and the three-point IpDTFT estimator [12] (called here the Fan estimator) are

compared to each other by means of simulations. Both versions (i.e., without and with signal windowing) of the Candan algorithm are considered, while the QS estimator is defined only for the rectangular window [29]. As suggested by the Authors, two iterations are performed in the AM and the Fan estimators, and the QS estimator is implemented through three iterations. The H-term MSD window and a fractional shift $p = 0.1$ bins have been used in the Fan estimator [12]. The expressions used for the considered frequency estimators are reported in In Table 1.

Monte Carlo simulations consider 100,000 runs of a complex-valued noisy sinewave with amplitude $A = 1$ p.u. and phase chosen at random in the range $[0, 2\pi)$ rad. The estimator Root Mean Square Error (*RMSE*) has been evaluated and compared with the square root of the CRLB, which is equal to $\left(\sigma_\nu^2\right)_{CR} \cong 3{\cdot}M/\left(2 \cdot \pi^2 \cdot \left(M^2 - 1\right) \cdot SNR\right)$ [15, 27]. In the following the results obtained by processing either unweighted or weighted signals are separately analysed.

4.1 Unweighted signal

Figure 2 shows the *RMSE*s of the LIpDTFT and the PIpDTFT frequency estimators and the corresponding $\sqrt{\text{CRLB}}$ as a function of *SNR* when $\nu = 2.3$ cycles are observed, $M = 16$ samples, and the fractional shift d_x is equal to 0.05 (Fig. 2a), 0.1 (Fig. 2b), and 0.3 (Fig. 2c) bins, respectively.

Figure 2 shows that the LIpDTFT frequency estimator almost attains the CRLB for all considered values of both *SNR* and fractional shift d_x, except when the *SNR* is below the breakdown threshold [27], which is equal to about 4 dB for the considered value of M. Conversely, the PIpDTFT frequency estimator ensures optimum accuracy only for small d_x values. It is worth noticing that the LIpDTFT frequency estimator almost attains the CRLB for all values of *SNR* when d_x is less than about 0.7 bins.

Figure 3 shows the *RMSE*s of the considered frequency estimators and the corresponding $\sqrt{\text{CRLB}}$ as a function of *SNR* when $\nu = 2.3$ cycles and the number of samples M is equal to 4 (Fig. 3a), 16 (Fig. 3b), and 64 (Fig. 3c). The fractional shift is $d_x = 0.1$ bins in both the PIpDTFT and the LIpDTFT algorithms.

Figure 3 shows that the LIpDTFT frequency estimator outperforms the others. It almost attains the CRLB for all considered values of M, except when the *SNRs* are either very low or very high and $M = 4$ samples. The PIpDTFT, the AM, and the Fan frequency estimators almost attains the CRLB when at least 64 samples are processed, even if the PIpDTFT estimator exhibits a better accuracy when fewer samples are available. The QS estimator almost attains the CRLB only if at least 64 samples are considered, and *SNR* is less than about 70 dB. The Candan estimator *RMSE* is close to the CRLB only for a limited range of *SNRs*, especially when few samples are available.

Figure 4 shows the Normalized *RMSE* (*NRMSE*), defined as the ratio between the *RMSE* and the CRLB of the most accurate frequency estimators, that is the AM, the Fan, the PIpDTFT, and the LIpDTFT estimator, as a function of the number of analyzed signal cycles ν, which varies in the range [0.1, 2] cycles with a step of 0.05 cycles. $SNR = 40$ dB, $M = 16$ samples, and $d_x = 0.1$ bins.

As we can see, the LIpDTFT frequency estimator has almost the same statistical efficiency as the Fan and the PIpDTFT estimators, except when coherent sampling

Table 1 The expressions for the used frequency estimators

Estimator	Estimator expression
classical two-point IpDFT estimator [24]	$\widetilde{\nu}_{2p} = l + \widetilde{\delta}_{2p} = l + Re\left\{\frac{\alpha(H+i-1)+H-i}{\alpha-1}\right\}$, with
	$\alpha \stackrel{\text{def}}{=} Y_w(l+i)/Y_w(l-1+i)$ and $i = \begin{cases} 0, & if\ \|Y_w(l)\| \leq \|Y_w(l-1)\| \\ 1, & if\ \|Y_w(l)\| > \|Y_w(l-1)\| \end{cases}$
Candan estimator [9]	$\widetilde{\nu}_{3p} = l + \widetilde{\delta}_{3p} = l + \gamma Re\left\{\frac{Y_w(l+1)-Y_w(l-1)}{Y_w(l-1)-2Y_w(l)+Y_w(l+1)}\right\}, \gamma = \frac{\tan(\pi/M)}{\pi/M}$
windowed Candan estimator [4, 23]	$\widetilde{\nu}_{3pw} = l + \widetilde{\delta}_1 + \widetilde{\delta}_2$, where $\widetilde{\delta}_1 = H \cdot Re\left\{\frac{Y_w(l+1)-Y_w(l-1)}{Y_w(l-1)-2Y_w(l)+Y_w(l+1)}\right\}$,
	$\widetilde{\delta}_2 = H \cdot Re\left\{\frac{Y_{w2}(l+1)-Y_{w2}(l-1)}{Y_{w2}(l-1)-2Y_{w2}(l)+Y_{w2}(l+1)}\right\}$,
	in which $y_{w2}(m) = y_w(m) \cdot exp\left(-j\frac{2\pi}{M}\widetilde{\delta}_1 m\right), m = 0, 1, .., M-1$
AM estimator [1, 6]	$\widetilde{\nu}_{AM} = l + \widetilde{\delta}_{i1} + \widetilde{\delta}_{i2}$,
	where $\widetilde{\delta}_{i1} = \frac{2H-1}{2} Re\left\{\frac{Y_w(l+0.5)+Y_w(l-0.5)}{Y_w(l+0.5)-Y_w(l-0.5)}\right\}$,
	$\widetilde{\delta}_{i2} = \frac{2H-1}{2} Re\left\{\frac{Y_w\left(l+\widetilde{\delta}_{i1}+0.5\right)+Y_w\left(l+\widetilde{\delta}_{i1}-0.5\right)}{Y_w\left(l+\widetilde{\delta}_{i1}+0.5\right)-Y_w\left(l+\widetilde{\delta}_{i1}-0.5\right)}\right\}$

Table 1 (continued)

Estimator	Estimator expression
QS estimator [29]	$\widetilde{\nu}_{QSE} = l + \sum_{i=1}^{Q} \widetilde{\delta}_i$, where $\widetilde{\delta}_1 = \frac{1}{c(q)} Re\left\{ \frac{Y_w(l+q) - Y_w(l-q)}{Y_w(l+q) - Y_w(l-q)} \right\}$, $c(q) = \frac{1-\pi q \cot(\pi q)}{q cos^2(\pi q)}$, $q = \frac{1}{\sqrt[3]{M}}$, $\widetilde{\delta}_k = \frac{1}{c(q)} Re\left\{ \frac{Y_w\left(l+\widetilde{\delta}_{k-1}+q\right) - Y_w\left(l+\widetilde{\delta}_{k-1}-q\right)}{Y_w\left(l+\widetilde{\delta}_{k-1}+q\right) - Y_w\left(l+\widetilde{\delta}_{k-1}-q\right)} \right\} + \widetilde{\delta}_{k-1}$, $k = 2, 3, \ldots, Q$
Fan estimator [12]	$\widetilde{\nu}_{Fan} = l + \widetilde{\delta}_{i1} + \widetilde{\delta}_{i2}$, where $\widetilde{\delta}_{i1} = \rho \Upsilon_1$, where $\rho = \frac{\cos(\pi p)\cdot a_0 - cos\left(\frac{\pi p}{M}\right)\cdot \sin(\pi p)\cdot \frac{1}{\pi}\cdot \sum_{h=0}^{H-1} (-1)^h \frac{p\cdot a_h}{p^2-h^2}}{\left\{ \left[\frac{1}{\pi}\cdot \sin(\pi p) + p\cdot \cos(\pi p) \right] \sum_{h=0}^{H-1} (-1)^h \frac{a_h}{p^2-h^2} - \frac{2p^2}{\pi}\cdot \sin(\pi p) \sum_{h=0}^{H-1} (-1)^h \frac{a_h}{\left(p^2-h^2\right)^2} \right\} \sin\left(\frac{\pi p}{M}\right)}$, with $p = 0.1$, and a_h, $h = 0, 1, \ldots, H-1$ are the window coefficients $\Upsilon_1 = \frac{[|Y_w(l+p)| - |Y_w(l-p)|]\sin\left(\frac{\pi p}{M}\right)}{[|Y_w(l+p)| + |Y_w(l-p)|]\cos\left(\frac{\pi p}{M}\right) - 2\cos(\pi p)|Y_w(l)|}$, $\widetilde{\delta}_{i2} = \rho \Upsilon_2$, where $\Upsilon_2 = \frac{\left[\left|Y_w\left(l+\widetilde{\delta}_{i1}+p\right)\right| - \left|Y_w\left(l+\widetilde{\delta}_{i1}-p\right)\right|\right]\sin\left(\frac{\pi p}{M}\right)}{\left[\left|Y_w\left(l+\widetilde{\delta}_{i1}+p\right)\right| + \left|Y_w\left(l+\widetilde{\delta}_{i1}-p\right)\right|\right]\cos\left(\frac{\pi p}{M}\right) - 2\cos(\pi p)\left|Y_w\left(l+\widetilde{\delta}_{i1}\right)\right|}$

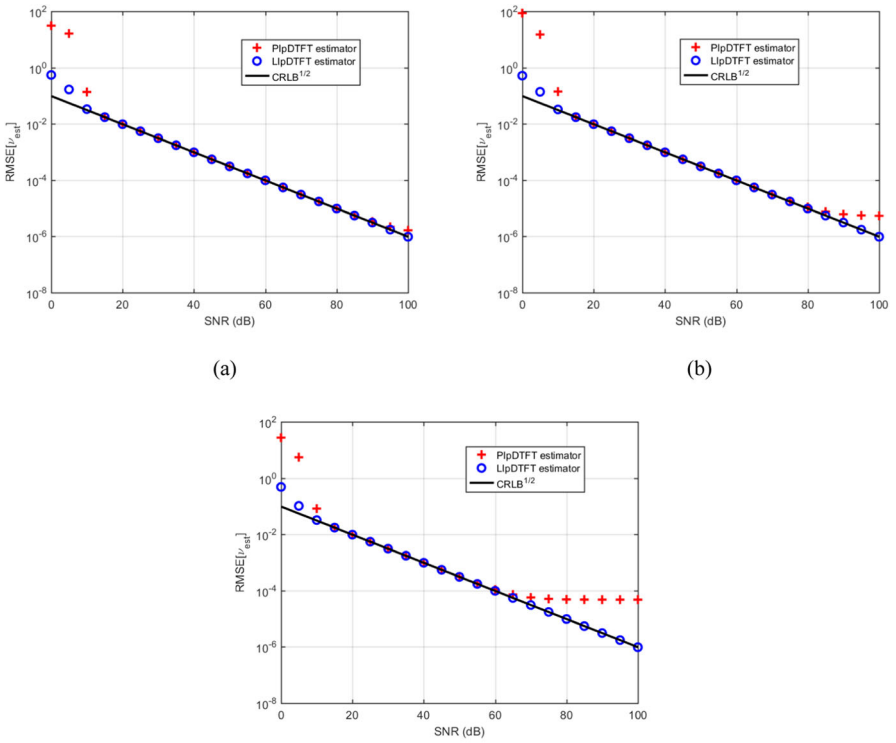

Fig. 2 Noisy complex-valued sinewaves: *RMSE* (in bins) of the PIpDTFT, and the LIpDTFT frequency estimators, and the $\sqrt{\text{CRLB}}$ versus *SNR* when $\nu = 2.3$ cycles when the fractional shift d_x is equal to 0.05 (**a**), 0.1 (**b**), and 0.3 (**c**) bins. For each *SNR* value 100,000 runs with sinewave phase chosen at random and $M = 16$ samples are considered

occurs where the LIpDTFT and the Fan estimators outperform the PIpDTFT estimator. Moreover, these three estimators outperform the AM estimator for all the considered values of ν.

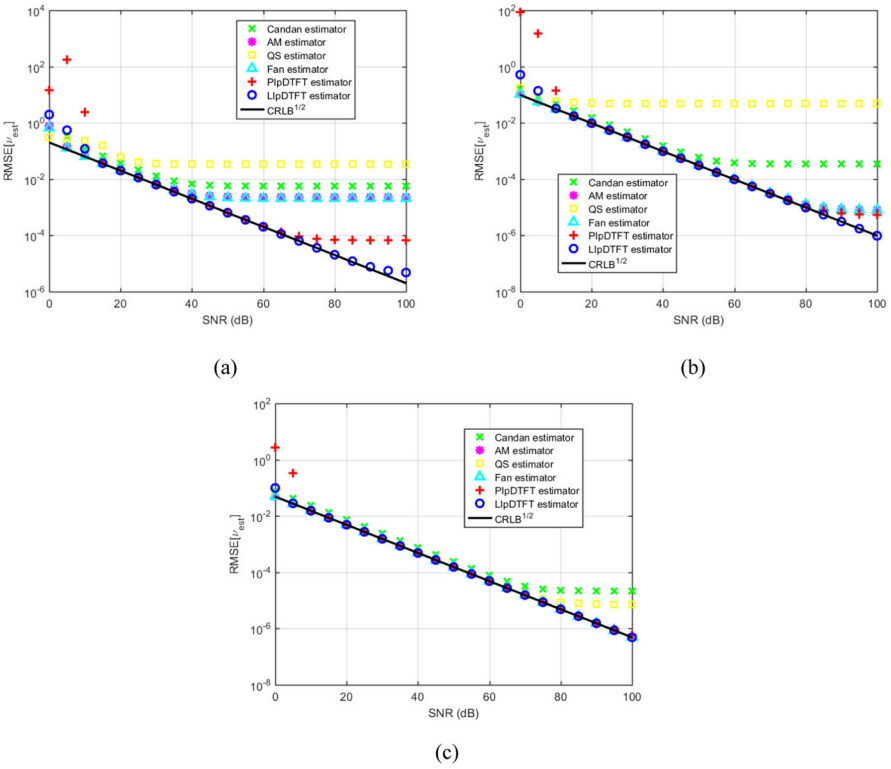

Fig. 3 Noisy complex-valued sinewaves: *RMSE* (in bins) of the Candan, the AM, the QS, the Fan, the PIpDTFT, and the LIpDTFT frequency estimators, and the $\sqrt{\text{CRLB}}$ versus *SNR* when $\nu = 2.3$ cycles. The fractional shift is $d_x = 0.1$ bins in both the PIpDTFT and the LIpDTFT estimators. For each *SNR* value 100,000 runs with sinewave phase chosen at random and $M = 4$ (**a**), 16 (**b**), and 64 (**c**) samples are considered

4.2 Weighted Signal

The Hann window is adopted to weight the acquired signal. Assuming the number of processed samples $M >> 1$, for that window we have [4]:

$$\widetilde{W}(d_x) = \frac{\sin(\pi d_x)}{2\pi d_x\left(1 - d_x^2\right)}, \tag{12}$$

from which, after some calculations, it follows that:

$$\widetilde{W}'(d_x) = \frac{\pi d_x \cos(\pi d_x)\left(1 - d_x^2\right) - \sin(\pi d_x)\left(1 - 3d_x^2\right)}{2\pi d_x^2\left(1 - d_x^2\right)^2}. \tag{13}$$

These expressions are used in the determination of the LIpDTFT frequency estimator (7) based on the Hann window even if small values of M are considered.

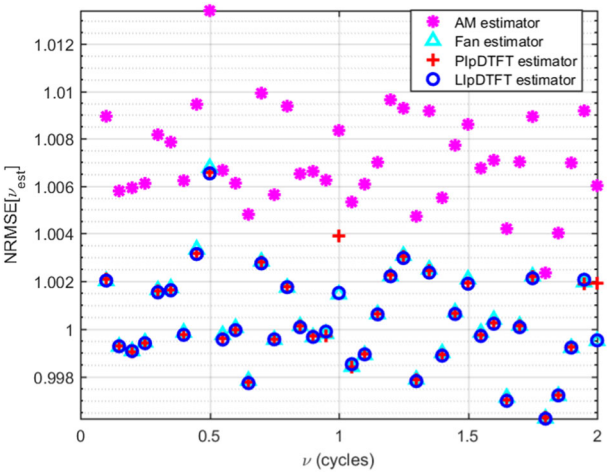

Fig. 4 Noisy complex-valued sinewaves: *NRMSE* of the AM, the Fan, the PIpDTFT, and the LIpDTFT frequency estimators versus ν when $SNR = 40$ dB. The fractional shift is $d_x = 0.1$ bins in both the PIpDTFT and the LIpDTFT estimators. For each value of ν 100,000 runs of $M = 16$ samples with sinewave phase chosen at random are considered

The QS estimator was not considered in the performed simulations since it holds only for the rectangular window [29].

Figure 5 shows the *NRMSE*s of the LIpDTFT and the PIpDTFT frequency estimators based on the Hann window as a function of *SNR* when $\nu = 2.3$ cycles are observed, $M = 16$ samples, and the fractional shift d_x is equal to 0.05 (Fig. 5a), 0.1 (Fig. 5b), and 0.3 (Fig. 5c) bins, respectively. As we can see, the LIpDTFT estimator slightly outperforms the PIpDTFT estimator, especially when the fractional shift d_x is not very small.

Figure 6 shows the *RMSE*s of the considered frequency estimators, all based on the Hann window, and the corresponding $\sqrt{\text{CRLB}}$ as a function of *SNR* when $\nu = 2.3$ cycles are observed and the number of samples M is equal to 4 (Fig. 6a), 8 (Fig. 6b), and 16 (Fig. 6c). In the PIpDTFT and LIpDTFT algorithm the fractional shift is $d_x = 0.1$ bins.

As it can be observed, when $M = 4$ samples the PIpDTFT frequency estimators outperforms the other estimators except for very low *SNR* values. For high *SNR* values the LIpDTFT estimator exhibits poor accuracy since the assumptions $M >> 1$ and $M >> d_x$ introduced to derive (13) no longer hold. However, when at least 8 samples are processed the *RMSEs* of all considered frequency estimators are close to the square root of the CRLB when *SNR* is not too small.

Figure 7 shows the *NRMSE* of the considered frequency estimators as a function of the number of analyzed signal cycles ν when $SNR = 40$ dB, $M = 16$ samples, and $d_x = 0.1$ bins. The parameter ν was varied in the range [0.1, 2] cycles with a step of 0.05 cycles. As we can see, the LIpDTFT, the PIpDTFT, and the Fan frequency estimators exhibit almost the same accuracy. They outperform the Candan and the

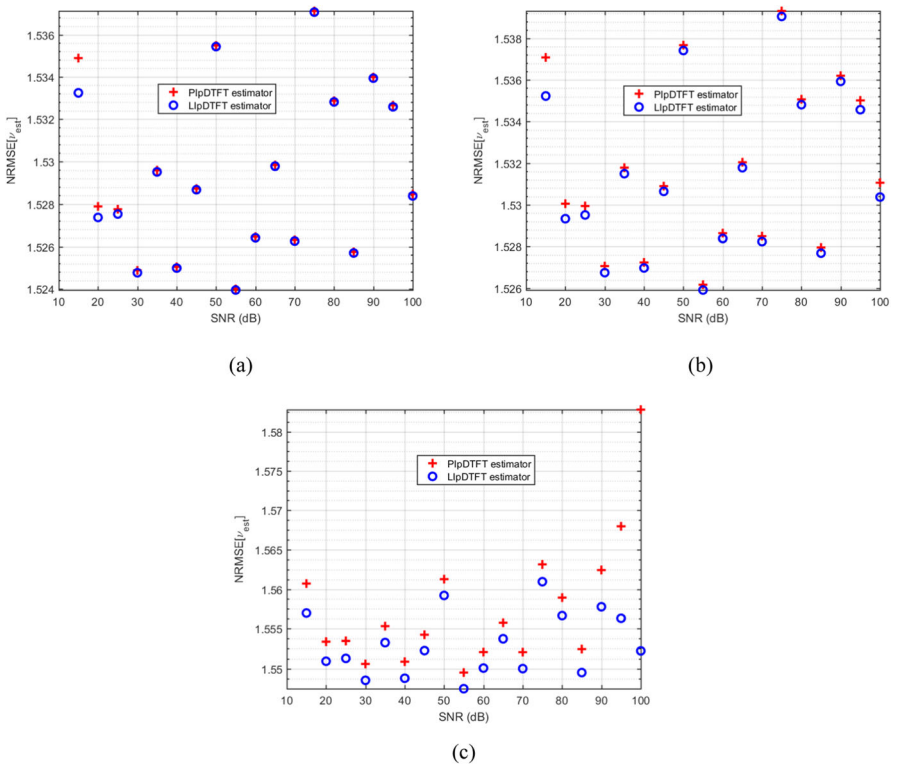

Fig. 5 Noisy complex-valued sinewaves: *NRMSE* of the PIpDTFT, and the LIpDTFT frequency estimators based on the Hann window versus *SNR* when $\nu = 2.3$ cycles. The fractional shift d_x is equal to 0.05 (**a**), 0.1 (**b**), and 0.3 (**c**) bins. For each *SNR* value 100,000 runs of $M = 16$ samples with sinewave phase chosen at random are considered

AM frequency estimators. Similar behavior has been observed for other values of the number of analyzed cycles ν.

The accuracies of all considered frequency estimators were compared to each other also when the acquired signal is affected by harmonics. Figure 8 shows the obtained *RMSE*s as a function of the number of acquired sinewave cycles ν when the sinewave is affected by a 2nd and a 3rd complex-valued harmonics of amplitude 0.1 p.u. and 0.05 p.u., respectively. Both the rectangular (Fig. 8a) and the Hann (Fig. 8b) windows are considered. The *SNR* is equal to 40 dB and 100,000 records of $M = 16$ samples with the phases of all components selected at random were processed. The observation interval length ν was varied in the range [0.1, 5] cycles with a step of 0.05 cycles and the fractional shift d_x is 0.1 bins in both the PIpDTFT and the LIpDTFT estimators.

Figure 8a shows that the LIpDTFT, the PIpDTFT, the Fan, and the AM frequency estimators exhibit almost the same *RMSE*s. Their values have a decreasing trend when ν increases and reach minima and maxima when the fractional frequency δ is close to 0.5 or 0 bins, respectively. On the whole, the accuracy of these estimators is better

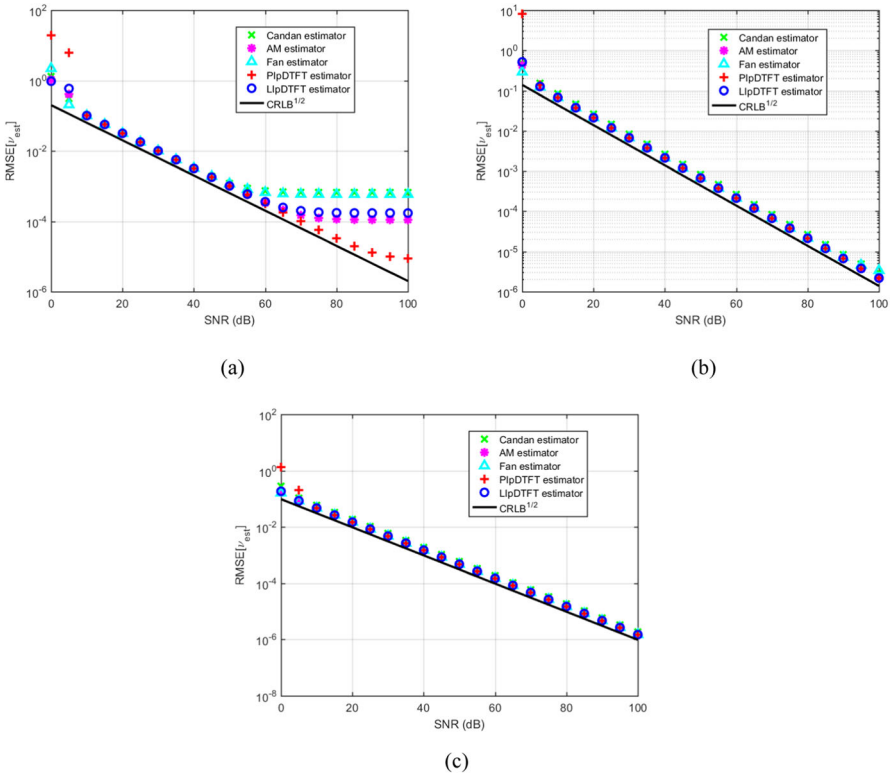

Fig. 6 Noisy complex-valued sinewaves: *RMSEs* of the Candan, the AM, the Fan, the PIpDTFT, and the LIpDTFT frequency estimators based on the Hann window, and the $\sqrt{\text{CRLB}}$ versus *SNR* when $\nu = 2.3$ cycles. The number of samples M is equal to 4 (**a**), 8 (**b**), and 16 (**c**). The fractional shift is $d_x = 0.1$ bins in both the PIpDTFT and the LIpDTFT estimators. For each value of *SNR* 100,000 runs of M samples with sinewave phase chosen at random are considered

than that of the QS estimator. Conversely, the Candan estimator often ensures better results when at least 2.5 cycles are observed.

Figure 8b shows that smaller *RMSE*s are obtained when the Hann window is used, thanks to its spectral leakage suppression capability. Also, the LIpDTFT, the PIpDTFT, the Fan, and the AM frequency estimators provide almost the same accuracy and, on the whole, it is smaller than that of the Candan estimator. When at least 4 cycles are observed, the *RMSE*s is almost constant since the contribution on the estimated frequency of the spectral interference from harmonics is dominated by the effect of wideband noise.

4.3 Computational Complexity Comparison

In the following the computational burdens required by the considered estimators are compared to each other. We assume that the number of analyzed sample M is a power

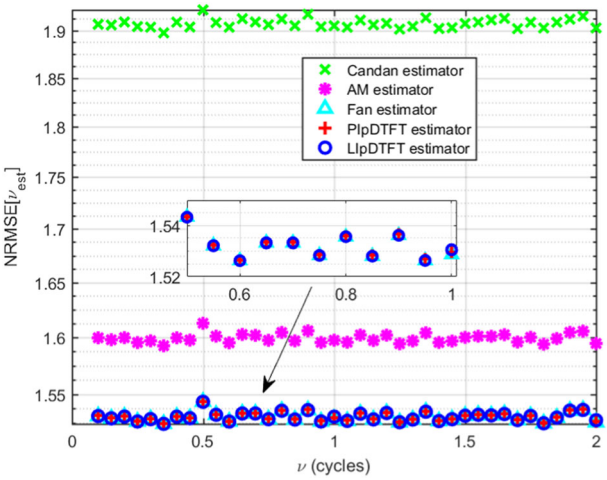

Fig. 7 Noisy complex-valued sinewaves: *NRMSEs* of the Candan, the AM, the Fan, the PIpDTFT, and the LIpDTFT frequency estimators based on the Hann window versus ν when $SNR = 40$ dB. The fractional shift is $d_X = 0.1$ bins in both the PIpDTFT and the LIpDTFT estimators. For each value of ν 100,000 runs of $M = 16$ samples with sinewave phase chosen at random are considered

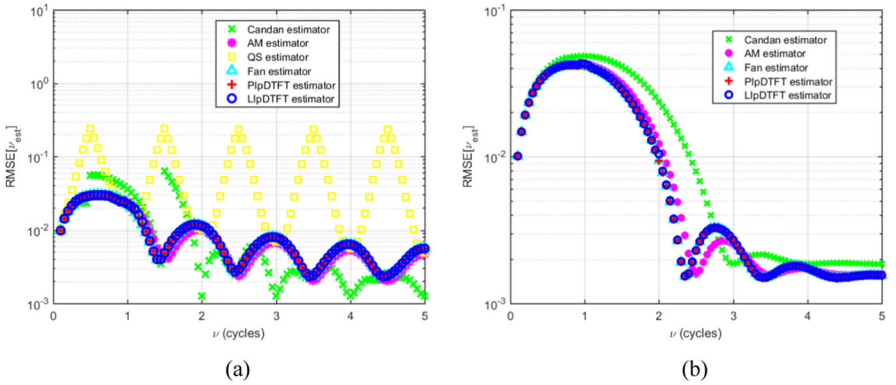

Fig. 8 Noisy and harmonically distorted complex-valued sinewaves: *NRMSE* of the considered frequency estimators versus the number of acquired sinewave cycles. **a** the Candan, the QS, the AM, the Fan, the PIpDTFT, and the LIpDTFT estimators based on the rectangular window; **b** the Candan, the AM, the Fan, the PIpDTFT, and the LIpDTFT estimators based on the Hann window. Signals affected by a 2nd and a 3rd complex-valued harmonics of amplitudes 0.1 p.u. and 0.05 p.u., respectively. $SNR = 40$ dB. For each value of ν 100,000 runs of $M = 16$ samples with the phases of all components chosen at random are considered

of 2 so that the DFT can be evaluated by applying a basic FFT algorithm, which requires $Mlog_2M$ complex-valued additions (CVAs) and $0.5M\log_2M$ complex-valued multiplications (CVMs) [18]. Thus, the DFT evaluation requires the computation of $3Mlog_2M$ real-valued additions (RVAs) and $2Mlog_2M$ real-valued multiplications (RVMs). In all estimators, the integer part l of the number of analyzed signal cycles is determined through a peak search procedure applied to the DFT square module,

Table 2 Number of RVAs and RVMs required by the considered algorithms. Rectangular window is assumed

Frequency estimator	RVAs	RVMs
Candan	$3M\log_2 M + M + 6$	$2M\log_2 M + 2\,M$
AM	$3M\log_2 M + 17\,M + 1$	$2M\log_2 M + 18\,M + 2$
QS	$3M\log_2 M + 25\,M + 2$	$2M\log_2 M + 24\,M + 3$
Fan	$3M\log_2 M + 21\,M + 2$	$2M\log_2 M + 22\,M + 18$
PIpDTFT	$3M\log_2 M + 13\,M + 5$	$2M\log_2 M + 14\,M + 7$
LIpDTFT	$3M\log_2 M + 9\,M + 5$	$2M\log_2 M + 10\,M + 7$

which implies M RVAs and 2 M RVMs. The calculation of the DTFT of a M-length data sequence implies $(M - 1)$ CVAs and M CVMs, which are equivalent to $(4M - 2)$ RVAs and $4M$ RVMs. Thus, when using the rectangular window, good estimates of the overall number of real-valued additions and multiplications required by the considered algorithms are those reported in Table 2.

Table 2 shows that the Candan estimator exhibits the lowest processing effort, but it has a high noise sensitivity, as shown in Fig. 3. The proposed LIpDTFT estimator requires the smallest processing effort among the estimators that ensure the highest frequency estimation accuracy. The same conclusion holds when windowing is used in the Candan, the AM, the Fan, the PIpDTFT, and the LIpDTFT algorithms.

5 Conclusions

In this paper a two-point interpolated DTFT (LIpDTFT) estimator for complex-valued sinewave frequency based on the linearization of the DTFT module behavior around the spectrum peak has been proposed. The interpolation points are located close to the initial frequency estimate, which is obtained through the classical two-point IpDFT algorithm. The LIpDTFT estimator exhibits a smaller interpolation error than the parabolic IpDTFT estimator. Moreover, when the rectangular window is adopted, the LIpDTFT estimator variance almost attains the CRLB even if a very small number of samples is analysed. In addition, the LIpDTFT estimator exhibits a better noise rejection capability than the Candan [8], the AM [1], the QS [29], and the Fan [12] frequency estimators when the number of analysed samples is very small. Conversely, when the signal is weighted by a cosine window and at least 8 samples are processed, the LIpDTFT algorithm exhibits the same accuracy as the Fan frequency estimator, and it outperforms the Candan frequency estimator. In addition, the proposed algorithm requires a smaller processing effort than all other considered algorithms capable to almost attain the CRLB. Thus, due to its characteristics, the proposed LIpDTFT algorithms can be advantageously employed in real-time frequency estimation of complex-valued noisy sinewaves of interest for application fields such as communications and radar signal processing.

Data Availability Data sharing is not applicable to this article as no datasets were generated or analyzed during the current study.

Declarations

Conflict of interest The authors declare that they have no conflict of interest or competing interests.

Appendix: Proof of Propositions 1 and 2

Proof of Proposition 1

Since the initial frequency estimate error $\Delta\nu_0$ is small, the Taylor's series expansion of $\widetilde{W}(\cdot)$ in (5) accurately expresses the DTFT sample values. By replacing (5) in (7), and using the approximation $(1 \pm x)^{-1} \cong 1 \mp x$, that holds for $|x| << 1$, after some algebra, the LIpDTFT frequency estimator interpolation error results:

$$\Delta\nu_{2l} \cong \left(\frac{\widetilde{W}''(d_x)}{2\widetilde{W}(d_x)} - \frac{\widetilde{W}'''(d_x)}{6\widetilde{W}'(d_x)}\right)\Delta^3\nu_0. \tag{A.1}$$

Since the fractional shift d_x is small, for the rectangular window we can write:

$$\widetilde{W}(d_x) \cong M\frac{\sin(\pi d_x)}{\pi d x} \cong M\left(1 - \frac{\pi^2 d_x^2}{6} + \frac{\pi^4 d_x^4}{120}\right), \tag{A.2}$$

$$\widetilde{W}'(d_x) \cong M\left[\frac{\cos(\pi d_x)}{d_x} - \frac{\sin(\pi d_x)}{\pi d_x^2}\right] \cong -\frac{\pi^2 d_x}{3}M\left(1 - \frac{\pi^2 d_x^2}{10}\right), \tag{A.3}$$

$$\widetilde{W}''(d_x) \cong -M\left[\frac{\pi\sin(\pi d_x)}{d_x} + \frac{2\cos(\pi d_x)}{d_x^2} - \frac{2\sin(\pi d_x)}{\pi d_x^3}\right] \cong -M\left(\frac{\pi^2}{3} - \frac{\pi^4 d_x^2}{10} + \frac{\pi^6 d_x^4}{120}\right), \tag{A.4}$$

and

$$\begin{aligned}\widetilde{W}'''(d_x) &\cong -M\left[\frac{\pi^2 cos(\pi d_x)}{d_x} - \frac{3\pi\sin(\pi d_x)}{d_x^2} - \frac{6\cos(\pi d_x)}{d_x^3} + \frac{6\sin(\pi d_x)}{\pi d_x^4}\right] \\ &\cong -\frac{\pi^4 d_x}{5}M\left(1 - \frac{\pi^2 d_x^2}{12}\right).\end{aligned} \tag{A.5}$$

where the following approximations have been used: $\sin(\pi d_x) \cong \pi d_x - \frac{\pi^3 d_x^3}{3!} + \frac{\pi^5 d_x^5}{5!}$ and $\cos(\pi d_x) \cong 1 - \frac{\pi^2 d_x^2}{2!} + \frac{\pi^4 d_x^4}{4!}$.

From (A.2)–(A.5) and applying the approximation $(1 \pm x)^{-1} \cong 1 \mp x$, $|x| << 1$, after some calculations it follows that:

$$\frac{\widetilde{W}''(d_x)}{2\widetilde{W}(d_x)} - \frac{\widetilde{W}'''(d_x)}{6\widetilde{W}'(d_x)} \cong -\frac{\pi^2}{15} + \frac{43\pi^4 d_x^2}{1800}. \tag{A.6}$$

in which the terms in d_x with degree higher than two have been neglected.

Finally, by replacing (A.6) into (A.1), (8) can be simply derived.

Proof of Proposition 2

The interpolation error of the parabolic frequency estimator $\widetilde{\nu}_{3p}$ is given by [5]:

$$\Delta\nu_{3p} \cong \left(1 - \frac{d_x}{2}\frac{\widetilde{W}'(d_x)}{\widetilde{W}(d_x) - M}\right)\Delta\nu_0. \tag{A.7}$$

By replacing (A.2) and (A.3) into (A.7), after simple calculations, (11) is obtained.

References

1. E. Aboutanios, B. Mulgrew, Iterative frequency estimation by interpolation on Fourier coefficients. IEEE Trans. Signal Process. **53**, 1237–1241 (2005). https://doi.org/10.1109/TSP.2005.843719
2. D. Belega, D. Petri, Sine-wave parameter estimation by interpolated DFT method based on new cosine windows with high interference rejection capability. Digital Signal Process. **33**, 60–70 (2014). https://doi.org/10.1016/j.dsp.2014.07.003
3. D. Belega, D. Petri, Effect of noise and harmonics on sine-wave frequency estimation by interpolated DFT algorithms based on few observed cycles. Signal Process. **140**, 207–218 (2017). https://doi.org/10.1016/j.sigpro.2017.05.021
4. D. Belega, D. Petri, Frequency estimation by two- or three-point interpolated Fourier algorithms based on cosine windows. Signal Process. **114**, 115–125 (2015). https://doi.org/10.1016/j.sigpro.2015.05.005
5. D. Belega, D. Petri, Unbiased sinewave frequency estimation by parabolic interpolation of DTFT samples, in *Proc. IEEE International Instrumentation and Measurement Technology Conference (I2MTC)* (Glasgow, United Kingdom, 2021). https://doi.org/10.1109/I2MTC50364.2021.9459910
6. D. Belega, D. Petri, D. Dallet, Accuracy of sinewave frequency estimation by an iterative interpolated DFT algorithm, in *Proc. IEEE International Instrumentation and Measurement Technology Conference (I2MTC)* (Pisa, Italy, 2015), pp. 1795–1800. https://doi.org/10.1109/I2MTC.2015.7151553
7. F. Bellili, Y. Selmi, S. Affes, A. Ghrayeb, A low-cost and robust maximum likelihood joint estimator for the doppler spread and CFO parameters over flat-fading Rayleigh channels. IEEE Trans. Commun. **65**, 3467–3478 (2017). https://doi.org/10.1109/TCOMM.2017.2697962
8. Ç. Candan, A method for fine resolution frequency estimation from three DFT samples. IEEE Signal Process. Lett. **18**, 351–354 (2011). https://doi.org/10.1109/LSP.2011.2136378
9. Ç. Candan, Analysis and further improvement of fine resolution frequency estimation method from three DFT samples. IEEE Signal Process. Lett. **20**, 913–916 (2013). https://doi.org/10.1109/LSP.2013.2273616
10. S. Djukanović, T. Popović, A. Mitrović, Precise sinusoid frequency estimation based on parabolic interpolation, in *Proc. IEEE Telecommunications ForumTelfor (TELFOR) Conference* (Belgrade, Serbia, 2016). https://doi.org/10.1109/TELFOR.2016.7818824

11. L. Fan, G.Q. Qi, J. Xing, J.Y. Jin, J.Y. Liu, Z.S. Wang, Accurate frequency estimator of sinusoid based on interpolation of FFT and DTFT. IEEE Access **8**, 44373–44380 (2020). https://doi.org/10.1109/ACCESS.2020.2977978
12. L. Fan, G. Qi, J. Liu, J. Jin, L. Liu, J. Xing, Frequency estimator of sinusoid by interpolated DFT method based on maximum sidelobe decay windows. Signal Process. **186**, 108125 (2021). https://doi.org/10.1016/j.sigpro.2021.108125
13. F.J. Harris, On the use of windows for harmonic analysis with the discrete Fourier transform. Proc. IEEE **66**, 51–83 (1978). https://doi.org/10.1109/PROC.1978.10837
14. E. Jacobsen, P. Kootsookos, Fast, accurate frequency estimators. IEEE Signal Process. Mag. **24**, 123–125 (2007). https://doi.org/10.1109/MSP.2007.361611
15. S.M. Kay, *Fundamentals of Statistical Signal Processing: Estimation Theory*, vol. 1 (Prentice-Hall, Upper Saddle River, 1993)
16. J.-R. Liao, S. Lo, Analytical solutions for frequency estimators by interpolation of DFT coefficients. Signal Process. **100**, 93–100 (2014). https://doi.org/10.1016/j.sigpro.2014.01.012
17. M.D. Macleod, Fast nearly ML estimation of the parameters of real or complex single tones or resolved multiple tones. IEEE Trans. Signal Process. **46**, 141–148 (1998). https://doi.org/10.1109/78.651200
18. D. Manolakis, V. Ingle, *Applied Digital Signal Processing* (Cambridge University Press, Cambridge, 2011)
19. H. Meyr, M. Moeneclaey, S.A. Fechtel, *Digital Communication Receivers—Synchronization, Channel Estimation and Signal Processing* (John Wiley & Sons, New York, 1998)
20. M. Morelli, M. Moretti, A.A. D'Amico, Single-tone frequency estimation by weighted least-squares interpolation of Fourier coefficients. IEEE Trans. Commun. **70**, 526–537 (2022). https://doi.org/10.1109/TCOMM.2021.3120735
21. A.H. Nuttall, Some windows with very good sidelobe behavior. IEEE Trans. Acoust. Speech Signal Process. **29**, 84–91 (1981). https://doi.org/10.1109/TASSP.1981.1163506
22. C. Offelli, D. Petri, The influence of windowing on the accuracy of multifrequency signal parameter estimation. IEEE Trans. Instrum. Meas. **41**, 256–261 (1992). https://doi.org/10.1109/19.137357
23. U. Orguner, Ç. Candan, A fine-resolution frequency estimator using an arbitrary number of DFT coefficients. Signal Process. **105**, 17–21 (2014). https://doi.org/10.1016/j.sigpro.2014.05.013
24. B.G. Quinn, Estimating frequency by interpolation using Fourier coefficients. IEEE Trans. Signal Process. **42**, 1264–1268 (1994). https://doi.org/10.1109/78.295186
25. M.A. Richards, *Fundamentals of Radar Signal Processing* (McGraw-Hill, New York, 2005)
26. D.C. Rife, G.A. Vincent, Use of the discrete Fourier transform in the measurement of frequencies and levels of tones. Bell Syst. Tech. J. **49**, 197–228 (1970). https://doi.org/10.1002/j.1538-7305.1970.tb01766.x
27. D.C. Rife, R.R. Boorstyn, Single tone parameter estimation from discrete-time observations. IEEE Trans. Inf. Theory **20**, 591–598 (1974). https://doi.org/10.1109/TIT.1974.1055282
28. S. Scherr, S. Ayhan, B. Fischbach, A. Bhutani, M. Pauli, T. Zwick, An efficient frequency and phase estimation algorithm with CRB performance for FMCW radar applications. IEEE Trans. Instrum. Meas. **64**, 1868–1875 (2015). https://doi.org/10.1109/TIM.2014.2381354
29. A. Serbes, Fast and efficient sinusoidal frequency estimation by using the DFT coefficients. IEEE Trans. Commun. **67**, 2333–2343 (2018). https://doi.org/10.1109/TCOMM.2018.2886355
30. H. Wu, H. Song, Y. Bai, L. Fan, J. Jin, J. Xing, Interpolated DFT algorithm for frequency estimation by using maximum sidelobe decay windows. IEEE Access **10**, 95478–95762 (2022). https://doi.org/10.1109/ACCESS.2022.3205350